

---

# A shotgun sampling solution for the common input problem in neural connectivity inference

---

Suraj Keshri, Eftychios Pnevmatikakis, Ari Pakman, Ben Shababo, Liam Paninski\*  
Statistics Department and Center for Theoretical Neuroscience  
Grossman Center for the Statistics of Mind  
Columbia University

## Abstract

Inferring connectivity in neuronal networks remains a key challenge in statistical neuroscience. The “common input” problem presents the major roadblock: it is difficult to reliably distinguish causal connections between pairs of observed neurons from correlations induced by common input from unobserved neurons. Since available recording techniques allow us to sample from only a small fraction of large networks simultaneously with sufficient temporal resolution, naive connectivity estimators that neglect these common input effects are highly biased. This work proposes a “shotgun” experimental design, in which we observe multiple subnetworks briefly, in a serial manner. We develop Bayesian methods based on generalized linear models (GLM) and “spike-and-slab” sparse priors to perform network inference given this type of data, and demonstrate in simulation that this shotgun experimental design can in fact eliminate the biases induced by common input effects. We find that observing as many different pairs of neurons as possible over the course of the serial experiment leads to the best inference results. We further develop methods for handling data with lower temporal resolution (as would be available via e.g. calcium fluorescence imaging). Finally, we develop approximate methods for performing inference in very large networks.

Advances in large-scale multi-neuronal recordings have made it possible to study the simultaneous activity of large ensembles of neurons. Experimentalists now routinely record from hundreds, or even thousands, of neurons simultaneously in a wide range of preparations. These new multineuronal recording techniques in principle provide the opportunity to discern the functional architecture of neuronal networks. As has been discussed at length elsewhere, the ability to accurately estimate large, possibly time-varying neural connectivity diagrams would open up an exciting new range of fundamental research questions in systems and computational neuroscience. Therefore, connectivity estimation can be considered one of the central problems in statistical neuroscience.

Perhaps the biggest challenge for inferring neural connectivity from functional data — and indeed in network analysis more generally — is the presence of hidden nodes which are not observed directly [1, 2, 3]. Despite swift progress in simultaneously recording activity in massive populations of neurons, it is still beyond the reach of current technology to monitor a complete network of spiking neurons at high temporal resolution (though see e.g. [4] for some impressive recent progress). Since estimation of functional connectivity relies on the analysis of the inputs to target neurons in relation to their observed spiking activity, the inability to monitor all inputs can result in persistent errors in the connectivity estimation due to model misspecification. More specifically, “common input” errors — in which correlations due to shared inputs from unobserved neurons are mistaken for direct, causal connections — plague most naive approaches to connectivity estimation. Developing

---

\*This work was supported by an NSF CAREER grant, a McKnight Scholar award, and by the U.S. Army Research Laboratory and the U. S. Army Research Office under contract number W911NF-12-1-0594. We thank D. Soudry for helpful conversations.

a robust approach for incorporating the latent effects of such unobserved neurons remains an area of active research in connectivity analysis [1, 2, 3].

In this paper we propose an experimental design which greatly ameliorates these common-input problems. The idea is simple: if we cannot observe all neurons in a network simultaneously, maybe we can instead observe many overlapping subnetworks in a serial manner over the course of a long experiment, and then use statistical techniques to patch the full estimated network back together<sup>1</sup>. (The analogy we have in mind is to “shotgun” genetic sequencing [6].) While it would be challenging to purposefully sample from many distinct but overlapping subnetworks using multi-electrode recording arrays, imaging methods (such as calcium fluorescence imaging [7, 8]) make this approach highly experimentally feasible.

The remainder of this paper focuses on the development of statistical methods for inferring connectivity given this type of “shotgun” data. A Bayesian approach is natural, due to the massive degree of missingness in the data (we assume that only a small fraction of the network is observed at any single time) and since a great deal of prior information about neuronal connectivity can be exploited here. We begin by describing the basic statistical model and how to sample from the associated posterior distributions. We then provide simulated results demonstrating that the shotgun experimental design can largely eliminate the biases induced by common input effects, as desired. We close by discussing approximate inference methods that scale to the case of very large networks, where standard Bayesian inference methods become infeasible.

### Generalized linear model

We use a rather standard discrete-time generalized linear network model (GLM) [9, 10, 11]:

$$p(\eta_{i,t} = 1) = f \left( \theta_i^T X_t + \sum_{j=1}^N W_{i,j} \eta_{j,t-1} + b_i \right) \quad (1)$$

where  $\eta_{i,t}$  is a binary variable indicating whether the  $i$ -th neuron spiked at time  $t$ ,  $f$  is a logistic function,  $X_t$  is a stimulus given to all the neurons at time  $t$ ,  $\theta_i$  is the spatio-temporal filter of neuron  $i$ ,  $b_i$  is a scalar offset, and  $W$  is the connectivity matrix we wish to infer. The diagonal elements  $W_{i,i}$  of the connectivity matrix are typically negative, corresponding to the post-spike filter accounting for the cell’s own (refractory) post-spike effects, while the off-diagonal terms  $W_{i,j}$  represent the connection weights from neuron  $j$  to neuron  $i$ . To simplify notation we have only included history effects with a single time lag; generalizing to multi-lag history effects is straightforward.

### Observation model

We assume that there are  $N$  neurons in the network, with a total of  $T$  timesteps. We assume that  $N$  is known; in the fluorescence imaging context, this implies that we can count all of the cells in the network. (We will discuss relaxations of this assumption below.) We further assume that only  $K < N$  of the neurons can be observed simultaneously at any time. We will study two cases. In the simplest, idealized case, we assume that we can observe the spiking of  $K$  neurons directly; i.e.,  $\eta_{j,t}$  is observed noiselessly for  $K$  values of the cell index  $j$  at any time step  $t$ . As noted above, it is not currently feasible to observe many different arbitrary subsets of neurons using electrical recording methods; therefore we also study a second case, in which we observe a noisy, convolved fluorescence signal instead of  $\eta_{j,t}$  directly. For this fluorescence signal we use the following first-order autoregressive (AR(1)) noisy convolution model [12]:

$$C_i(t) = \gamma_i C_i(t-1) + A_i \eta_{i,t} + d_i \quad (2)$$

$$Y_i(t) = C_i(t) + \sigma_i \epsilon_i(t), \quad \epsilon_i(t) \sim \mathcal{N}(0, 1). \quad (3)$$

Here  $Y_i(t)$  is the observable signal from neuron  $i$  at time  $t$ ;  $\mathcal{N}(0, 1)$  denotes the standard normal distribution;  $C_i(t)$  is a latent variable ( $C$  stands for “calcium” in this context) that represents the output of the AR(1) filter in eq. 2;  $d_i$  denotes this filter’s baseline,  $A_i$  denotes the gain, and  $\gamma_i$  sets the timescale. (Again, we have chosen the simplest reasonable model for  $Y_i(t)$  here; it is straightforward to generalize the analytical methods described below to more complex models.) As in the

<sup>1</sup>See also [5], who independently recently proposed a similar approach, using an approximate linear-Gaussian model for neuronal dynamics which is simpler than the model we discuss here.

direct observation case, we assume that only  $K$  of the possible  $N$  fluorescence signals  $Y_i(t)$  can be observed at any time  $t$ . For simplicity we will assume that the filter parameters  $(\gamma_i, A_i, d_i, \sigma_i)$  have been estimated (e.g., via the methods discussed in [12] and references therein), and are therefore held fixed during the estimation of the GLM parameters  $(W, \theta_i, b_i)$ ; this can be generalized as well.

### Sparse priors on the connectivity parameters

A great deal of prior information is available concerning both connection probabilities and synaptic weight distributions as a function of cell location and identity [13]. In addition, cutting edge labeling and tissue preparation methods such as Brainbow [14] and CLARITY [15] are beginning to provide rich anatomical data about “potential connectivity” (e.g., the degree of coarse spatial overlap between a given set of dendrites and axons) that can be incorporated into these priors. Exploiting this prior information can greatly improve inference quality, as demonstrated in a number of previous network inference papers [11, 12].

The most popular approach for incorporating prior information about sparsity is to use a LASSO prior [16]:  $p(W) \propto \prod_{ij} \exp(-|\lambda_{i,j} W_{i,j}|)$ , for some set of sparsity parameters  $\lambda_{i,j}$ . This prior has a number of advantages: the resulting log-posterior of  $W$  (given the full spike train  $\eta$  and the other system parameters) turns out to be a concave function of  $W$  (as we will discuss at more length in the next section), and the maximizer of this posterior,  $\hat{W}_{MAP}$  is often sparse, i.e., many values of  $\hat{W}_{MAP}$  are zero. These two facts greatly facilitate expectation-maximization (EM) based approaches for estimating  $W$  from incomplete data, as emphasized previously in [12].

In practice we found that an alternative fully-Bayesian approach led to a more flexible and accurate inference framework, for reasons discussed at more length in the next section. Specifically, we use a “spike-and-slab” prior model for  $W$ . These models have received a good deal of attention in the statistics literature [17] and are now enjoying a resurgence in the machine learning literature [18]; see also [10] for a successful application of a similar model to a neural connectivity problem. The spike-and-slab prior can be constructed using a binary indicator matrix  $Z$  to indicate whether weights in the matrix  $W$  are zero or not. Each neuron pair  $i, j$  has a corresponding Bernoulli indicator variable  $Z_{i,j}$ , with  $p(Z_{i,j} = 1) = \pi_{i,j}$  for some  $N \times N$  parameter matrix  $\pi$ . The full model is:

$$p(Z|\pi) = \prod_{ij} \mathcal{B}(Z_{i,j}|\pi_{i,j}) = \prod_{ij} \pi_{i,j}^{Z_{i,j}} (1 - \pi_{i,j})^{1-Z_{i,j}} \quad (4)$$

$$p(W|Z, \mu, V) = \prod_{i,j} \mathcal{N}(W_{i,j}|Z_{i,j}\mu_{i,j}, Z_{i,j}V_{i,j}^2). \quad (5)$$

In words: when  $Z_{i,j}$  is zero, the corresponding distribution of  $W_{i,j}$  is a delta function (a “spike”) with all of its mass at zero; when  $Z_{i,j}$  is one,  $W_{i,j}$  is normally distributed with mean  $\mu_{i,j}$  and variance  $V_{i,j}$ . Following the discussion above, we assume that we have a priori estimates for the hyperparameters  $\pi, \mu$ , and  $V$ ; it is also possible to infer hierarchical models for these parameters using standard posterior sampling or EM approaches, though for simplicity we skip the details here. Finally, note that if information about neuronal cell types is available (for example, via fluorescent markers), then we can replace the normal distribution in eq. 5 with a truncated normal (or log-normal [13]) to enforce the positivity (negativity) of the corresponding excitatory (inhibitory) weight.

### Inference

The two classical approaches for parameter estimation in this type of latent-variable setting are EM — which provides an estimator that locally optimizes the posterior of  $W$  given the observed data — and Markov chain Monte Carlo (MCMC) sampling from this posterior. We experimented with both approaches, and will briefly describe both in turn.

*Expectation maximization:* The EM approach is similar to the methods discussed in [2, 12]. The E step requires the computation of an integral<sup>2</sup> over  $p(\eta|\eta_{obs}, W)$  or  $p(\eta|Y, W)$ ; this integral is high-dimensional and not analytically tractable, so we resort to MCMC methods to sample from these

<sup>2</sup>A comment on notation: we will be interested in posteriors such as  $p(\eta|Y, W, \{\theta_i\}, X, \{b_i\}, \{\gamma_i\}, \{A_i\}, \{d_i\}, \pi, \mu, \sigma^2)$ . Our focus here is on estimating  $W$ , so to keep the notation manageable we’ll suppress the extra parameters and just write  $p(\eta|Y, W)$  (in the fluorescence observation setting) and  $p(\eta|\eta_{obs}, W)$  (when the subset  $\eta_{obs}$  is observed directly).

posterior distributions. Since the  $\eta_{i,t}$  variables are binary, Gibbs sampling is a natural approach. Specifically, we used the improved Metropolized Gibbs sampler described in [19]. This sampler is quite simple and is extremely parallelizable in this setting, because the graphical model representing the posterior  $p(\eta|\eta_{obs}, W)$  is extremely local:  $\eta_{.,t}$  is conditionally independent of  $\eta_{.,t+2}$  given  $\eta_{.,t+1}$  (since the spiking at time  $t$  only directly affects the spiking in the next time step; i.e., model (1) can be considered a Markov chain in  $\eta_{.,t}$ ). Therefore we can alternately sample the spiking vectors  $\eta_{.,t}$  at all odd times  $t$  completely in parallel, and then similarly for the even times. (A similar locality property holds for  $p(\eta|Y, W)$ , due to the finite effective width of the AR(1) filter; in this case,  $\eta_{.,t}$  is conditionally independent of and can therefore be sampled in parallel with  $\eta_{.,t+c}$ , where  $c$  is a sufficiently large multiple of the timescale of the filter decay, as set by the  $\gamma$  parameter in eq. (2).) We note that more sophisticated sampling methods have been developed for this type of problem [20]; these specialized methods are significantly more efficient if implemented serially, but do not parallelize as well as the simple Gibbs-based approach we used here.

One major improvement should be noted: we found that in most cases it was not necessary to take many samples from the posterior; for large enough network sizes  $N$  (and for correspondingly long experimental times  $T$ ),  $\eta$  is large enough that a single sample contains enough information to adequately estimate the necessary sufficient statistics in the E step. See [21] for further discussion.

As emphasized above and in [2, 12], the M step under a LASSO prior reduces to a sequence of separable convex GLM optimization problems that can be solved in parallel (one problem per neuron). Stochastic gradient ascent methods are also applicable here, though we found that taking full M steps often led to better performance (largely because of the availability of very fast and mature software for LASSO-penalized GLM estimation). Due to space constraints, we skip the details of the M-step here, and refer the reader to [2, 12].

*MCMC sampling from  $W$* : As noted above, the EM approach with the LASSO prior has some attractive features, largely due to the convex structure of the M step and the sparsity-promoting nature of the LASSO prior. However, similar to the results in [18], we found the fully Bayesian MCMC spike-and-slab approach superior here. The main advantage of the MCMC spike-and-slab approach is that samples from the posterior suffer from less shrinkage than the LASSO maximum a posteriori (MAP) estimator: if the nonzero elements of  $W$  are identified fairly well, then samples from the spike-and-slab posterior give fairly unbiased estimators of the true weights  $W$ , while the LASSO MAP estimator displays a strong bias towards zero, even for the optimal choice of the sparsity parameters  $\lambda$ . We omit the figures demonstrating these effects to save space, but see e.g. [12] for further discussion of this issue. We should also note that the MCMC approach offers somewhat simpler methods for hyperparameter selection (via sampling from the hyperparameter posterior), and easier incorporation into larger hierarchical models that can incorporate richer prior information about the network and enable proper sharing of information across networks. Finally, Bayesian experimental design methods require a full posterior (or at least some approximation thereof), and the MAP solution does not provide this.

To sample from the posterior of  $W$ , we use a Gibbs approach to sample jointly from  $p(\eta, W|\eta_{obs})$  (or  $p(\eta, W|Y)$ ): first sample  $\eta$  given the observed data and the current sample from  $W$ , and then sample  $W$  given  $\eta$ . The first step uses exactly the same algorithm as the E step described above, in which we draw one sample from the posterior of  $\eta$  given the observed data and an estimated  $W$ . For the second step, to sample  $W$  given  $\eta$ , we first note that the posterior factorizes:  $p(W|\eta) = \prod_i p(W_{i.,}|\eta)$ . Thus, we can sample from each  $p(W_{i.,}|\eta)$  in parallel. To sample from  $p(W_{i.,}|\eta)$ , we follow the approach of [10, 18] and simply Gibbs sample, one element  $W_{i,j}$  at a time. This requires a marginalization over the binary variables  $Z_{i,j}$  that determine whether  $W_{i,j}$  is zero or not (i.e., in the spike or in the slab); as discussed in [18], this requires the computation of some one-dimensional integrals. In our case these integrands are log-concave and therefore unimodal; like [18], we found that Laplace approximations of these integrals led to excellent proposals for a Metropolis-Hastings-within-Gibbs sampler of these variables.

## Results

Figure 1 illustrates our major results. In this case the network size  $N = 50$ ; similar results were obtained with larger networks, but visualizing the results becomes harder for larger  $N$ . The top panel shows the true  $W$  used in the simulations, while each of the five lower rows illustrates the

results obtained using a different observation scheme. All results shown here were obtained using the MCMC spike-and-slab sampler. The left column shows the inferred  $\hat{W}$  (in this case, a sample from the posterior after a sufficient burn-in period); the middle column is a scatterplot of the true weights  $W$  against the estimated  $\hat{W}$  (each dot corresponds to a single element  $W_{i,j}$ , and the diagonal line indicates the identity line); the right column illustrates the sampling scheme used by plotting  $\eta_{obs}$  in red and the unobserved elements  $\eta_{i,t}$  in blue. Each simulation used the same true  $\eta$ ; the only differences were in which subsets of  $\eta$  were observed (as indicated in the right panels). We focus on the case that  $\eta_{obs}$  is observed noiselessly; similar results are obtained in the case of fluorescence observations, assuming sufficiently high signal-to-noise and temporal resolution [12], as will be described in detail in a longer version of this work.

In the results shown in the first row, the full  $\eta$  was observed.  $T$  was chosen so that inference using the fully-observed spike data  $\eta$  would be accurate; as seen here, there is a good correspondence between  $\hat{W}$  and  $W$ . (Note that there is an overrepresentation of zero elements in both the true and inferred  $W$ , due to the spike-and-slab prior.)

The second row illustrates that the shotgun sampler works as desired: at any time  $t$ , only  $K = 10$  out of  $N = 50$  neurons were observed. We chose 60 random  $K$ -subsets (ensuring that each of the  $N(N - 1)/2$  neuron pairs  $(i, j)$  appeared at least once), and observed each subset for  $T/60$  timesteps. We see that the inference quality in this case is comparable to the fully-observed case.

The third row illustrates a “restricted” shotgun sampler. In this case, we keep  $K = 10$ , as before, but restrict the subsets to sample from “contiguous” blocks of neurons. The idea is to examine the impact of imaging only spatially contiguous subsets of neurons, as may be more convenient in many fluorescence imaging setups. (In these simulations, there was no spatial structure, and we just defined continuity in terms of the indices  $1 \leq i \leq N$ .) In this case, “distant” neural pairs  $(i, j)$  (specifically, those for which  $|i - j| > K$ , with appropriate circular boundary conditions) are never observed simultaneously. We see that the inference quality suffers in this setting; this emphasizes the importance of random-access imaging methods [7, 8] in this context.

The last two rows require a bit more explanation of the true connectivity  $W$ . We chose this  $W$  to illustrate a “worst-case” common input condition. Note that the upper-left third of  $W$  is diagonal: i.e., neurons  $i = 1, \dots, 17$  share no connections to each other, other than the self-connection terms  $W_{i,i}$ . However, we have seeded this  $W$  with many common-input motifs, in which neurons  $i$  and  $j$  (with  $i, j \leq 17$ ) both receive common input from neurons  $k$  with  $k > 17$ . Therefore we should infer a diagonal  $17 \times 17$  upper-left submatrix, but if common noise is problematic then we will “hallucinate” many nonexistent connections (i.e., off-diagonal terms) in this submatrix. The fourth row illustrates exactly this phenomenon. In this case, we observe the first  $K = 17$  neurons and proceed with inference under the mistaken assumption that all of the neurons in the network have been observed (i.e., that  $K = N$ ). The resulting estimates are strongly corrupted by the common input effects described above. The fifth row is based on the same data, but using the correct value of  $N$  (i.e., acknowledging that only  $K = 17$  out of  $N = 50$  neurons were observed). Inference performance in this case is improved, but is still significantly worse than in either of the shotgun simulations discussed above, even when attention is restricted to the observed  $17 \times 17$  submatrix.

## Large scale approaches

The results above illustrate the potential power of the proposed shotgun network inference methods. The next challenge is to scale the inference methods to very large network sizes  $N$ , where even highly parallelized implementations of the MCMC approaches presented here will become infeasible. Luckily, standard probabilistic approximations can be exploited in the limit of large  $N$ .

## Variational Bayes and a connection to maximum entropy models

Variational Bayes (VB) methods have become quite popular for performing approximate inference in large graphical models. The basic idea is to approximate the difficult posterior distribution  $p$  of interest (here, the posteriors of  $\eta$  and  $W$  given the observed data, along with the necessary hyperparameters) with a simpler distribution  $q$  of factorized form. This approximate distribution  $q$  may be defined by a few parameters  $\phi$ ; thus, the goal is to choose the parameters  $\phi$  to minimize the Kullback-Leibler (KL) divergence,  $\min_{\phi} D_{KL}(q_{\phi}; p)$ .

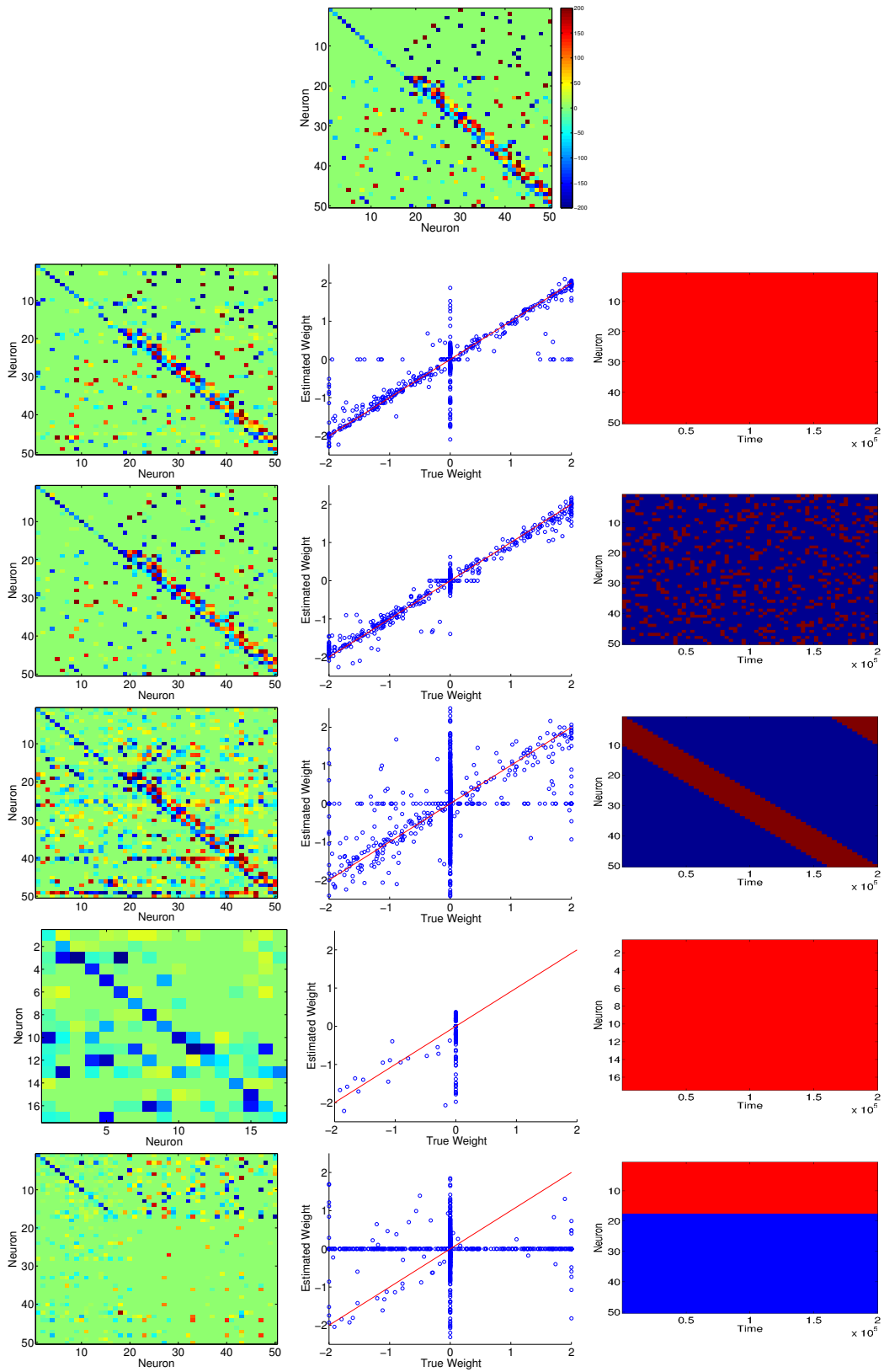


Figure 1: See Results text for full description.

In our context, we would like, for example, to replace  $p(\eta|W, \eta_{obs})$  with a more tractable approximation. One reasonable starting point is to define the fully-factorized Bernoulli approximation

$$q(\eta|\phi) \propto \prod_{i,t} q(\eta_{i,t}|\phi_{i,t}) = \prod_{i,t} \mathcal{B}(\eta_{i,t}|\phi_{i,t}), \quad (6)$$

where the product is restricted to unobserved indices  $i, t$ ; for observed indices,  $q$  places a delta mass on the observed data. The parameters  $\phi_{i,t}$  here define the firing probability of each neuron  $i$  at time  $t$ ; clearly, this approximation discards a good deal of information about correlations in the network, but the hope is that by choosing the vector  $\phi$  that minimizes the KL divergence between  $p$  and  $q$ , some of this important information might be retained, allowing the inference to proceed successfully.

There is a standard procedure for iteratively computing the (locally) KL-optimal  $\phi$  in this setting; see e.g. [22] for details. Abbreviate  $\nu_{i,t} = \theta_i^T X_t + \sum_{j=1}^N W_{i,j} \eta_{j,t-1} + b_i$ . In our setting we need to compute expectations of the form

$$E_{q_{\setminus i}} \log p(\eta|\eta_{obs}, W) \equiv E_{\prod_{(j,s) \neq (i,t)} q(\eta_{j,s}|\phi_{j,s})} \left[ \eta_{i,t} \nu_{i,t} + \sum_{k=1}^N g(\nu_{k,t+1}) \right] + const., \quad (7)$$

with  $g(\cdot) = -\log(1 + \exp(\cdot))$ . The first term in the brackets requires the computation of just a few moments of  $q$ , and is therefore straightforward. However, to take the expectation of the second term we need to compute a sum (in the definition of  $\nu_{i,t}$ ) that scales exponentially in the number of unobserved neurons, and is therefore intractable. However, when  $N$  is sufficiently large we can invoke the central limit theorem (CLT) to approximate the sum  $\sum_{j=1}^N W_{k,j} \eta_{j,t}$  within  $g(\cdot)$ :

$$E[g(\nu_{k,t+1})] = E \left[ g \left( \theta_k^T X_{t+1} + \sum_{j=1}^N W_{k,j} \eta_{j,t} + b_k \right) \right] \approx E_{z \sim \mathcal{N}(\mu_z, \sigma_z^2)} [g(z)] \equiv F(\mu_z, \sigma_z^2), \quad (8)$$

where  $z$  is a Gaussian variable with mean and variance

$$\mu_z = \theta_k^T X_{t+1} + W_{k,i} \eta_{i,t} + \sum_{j \neq i} W_{k,j} \phi_{j,t} + b_k; \quad \sigma_z^2 = \sum_{j \neq i} W_{k,j}^2 \phi_{j,t} (1 - \phi_{j,t}). \quad (9)$$

(See e.g. [23, 24] for similar approximations.) The function  $F(\cdot, \cdot)$  depends only on two variables  $(\mu_z, \sigma_z^2)$ , and can therefore be precomputed and cached as a special function (or approximated further, e.g. via a Taylor series), making these approximate VB iterations tractable in this setting. The per-iteration cost can be improved further if we spend more time updating parameters in timebins  $(i, t)$  near bins containing observed data (since more distant values of  $\phi_{i,t}$  can be safely set to their prior mean; proximity here is measured in terms of the graphical model corresponding to eq. 1). The VB iterations can also be parallelized in exactly the same manner as the Gibbs sampler discussed above. Further simplifications are possible if we use a subsampling or law of large numbers approach to approximate the large sums in eq. 7, or make some Taylor approximations of  $g(\cdot)$  and/or  $F(\cdot)$ ; see [25] for details of related approaches, and [26] for further background. Further work is necessary to more thoroughly explore these various possibilities.

Once the KL-optimal factorized  $q$  is in hand, we can proceed in a few different directions. Integrating (or rather, summing over)  $q$  is straightforward; we thus have a tool for approximating the marginal likelihood of  $\eta_{obs}$  (marginalized over the hidden spiking variables), and we can plug this approximate marginal likelihood directly into the spike-and-slab sampler for  $W$  described above. Alternatively, VB approximations to the spike-and-slab posterior are available as well [27]; we will discuss these further below. Finally, we can also trivially sample from  $q$ . For example, in the case of fluorescence observations  $Y$  (instead of the direct observations  $\eta_{obs}$  we have considered thus far in this section), we can Gibbs sample, alternating between drawing a new  $\eta_{obs}$  given  $Y$  and then running the VB approximation for the unobserved spiking data, and drawing a sample from the resulting factorized density.

### Expected loglikelihood approximation

A more direct approximation can be constructed using the ‘‘expected loglikelihood’’ methods discussed in [28, 29, 30]. First, note that, as usual, the logistic regression spiking model can be approximated as a Poisson regression model when the timebin size is sufficiently small. Second, when  $N$  is

sufficiently large, we can apply a central limit theorem argument to approximate the sum over  $N$  in the log firing rate  $\nu_{i,t}$  as Gaussian. Finally, recall from [28, 29, 30] that the profile expected loglikelihood (where the expectation is taken over this approximately Gaussian variable  $\nu_{i,t}$ ) in the Poisson regression model turns out to be quadratic as a function of the regression parameters. Putting these three ideas together, we find that, when  $N$  is sufficiently large, the logistic regression likelihood can be approximated by a standard linear-Gaussian regression likelihood.

The sufficient statistics for this approximate regression model are simply the first and second moments of the terms comprising  $\nu_{i,t}$ ; specifically, we have to estimate the mean and covariance of the covariates  $(\eta_t, X_t)$ , along with the pairwise cross-covariance of  $(\eta_t, X_t)$  with the response variable  $\eta_{t+1}$ . We can estimate these sample moments using only data for which all elements of the moments are available; i.e., to approximate a moment  $E(\eta_{i,t}\eta_{j,t-1})$ , simply take a (properly normalized) sum over those time points for which neuron  $i$  is observed at time  $t$  and neuron  $j$  is observed at time  $t-1$ . (Note that this is not necessarily possible if the collection of observed subsets is insufficiently rich; c.f. the third and fifth rows of Fig. 1.) The major advantage of this approach is that we do not have to spend any time inferring the missing  $\eta$  data<sup>3</sup>; the disadvantage is that we may lose some statistical efficiency by ignoring prior information about the probabilities of spiking in the unobserved bins. (That said, our numerical experiments indicate that in many cases the unobserved bins provide much less information than the observed bins, and highly accurate estimates can be obtained without any inference of the unobserved spiking probabilities.)

Once the required covariances have been estimated, one can apply one’s preferred sparse linear regression technique; we found the VB spike-and-slab method of [27] to be effective here. The two steps of the code (computation of the sufficient statistics, then estimation of the linear regression model for each  $W_{i,\cdot}$ ) are highly parallelizable and can furthermore be implemented in an online manner, in the context of real-time adaptive experimental design. Applied to a network of size  $N = 1000$  (with  $K/N = 0.2$  and  $T = 2 \cdot 10^5$  time steps), this method provides accurate inference in about 10 minutes (using a non-optimized, serial implementation of the code on a laptop); optimized, parallel implementations will scale easily to networks an order of magnitude larger. Finally, in cases where more computational resources are available it is easy to form a weighted average of the estimates provided by any of the three methods discussed here, with the weight on the Gibbs (or VB) contribution proportional to the number of sampled missing data time bins  $t$ . This approach is attractive because it allows us to tradeoff between computation time and accuracy in a straightforward manner: if we are severely limited computationally then we can just use the cheap expected loglikelihood approximation and not sample at all; if we have more computation time then we can sample from (or apply VB to) more unobserved time bins  $t$ .

## Future work

A number of further directions are available for future work. First, we have assumed that  $N$  is known. In cases where this assumption is unreasonable, we can augment the basic GLM to incorporate latent lumped Gaussian terms (as in [31]), or simply add some unobserved neurons to the network and run the inference including these terms [2]; this can significantly improve estimation accuracy (c.f. Fig. 1, bottom). Second, a number of alternative approximations are available involving the posteriors discussed here [1, 31, 26]. It will be quite valuable to more systematically compare these approaches. In particular, there is an important experimental design question here: what sampling schedule for observing  $\eta_{obs}$  provides the most information about  $W$ ? One starting point is to replace the GLM spiking model (1) with a simpler Gaussian observation model. In this case, our model becomes a Kalman filter, in which exact computations are possible. See [5] for a detailed discussion of this approach, with a promising application to imaging data from somatosensory cortex. We are currently examining this approximation to guide experimental design, using ideas similar to those discussed in [32].

---

<sup>3</sup>There is also a technical assumption here, specifically that the unobserved data are missing completely at random, i.e., all required expectations remain unchanged when taken under just the observed fraction  $\eta_{obs}$ . This assumption is very reasonable here, since we are not choosing the observed neural subset at time  $t$  based on how the neurons are firing at this time.



## References

- [1] D. Nykamp, “A mathematical framework for inferring connectivity in probabilistic neuronal networks,” *Mathematical Biosciences*, vol. 205, pp. 204–251, 2007.
- [2] J. Pillow and P. Latham, “Neural characterization in partially observed populations of spiking neurons,” *NIPS*, 2007.
- [3] M. Vidne *et al.*, “Modeling the impact of common noise inputs on the network activity of retinal ganglion cells,” *Journal of Computational Neuroscience*, vol. 33, no. 1, pp. 97–121, 2012.
- [4] M. Ahrens, M. Orger, D. Robson, J. Li, and P. Keller, “Whole-brain functional imaging at cellular resolution using light-sheet microscopy,” *Nature Methods*, vol. 10, pp. 413–420, 2013.
- [5] S. Turaga, L. Buesing, A. Packer, H. Dalgleish, N. Pettit, M. Hausser, and J. Macke, “Inferring neural population dynamics from multiple partial recordings of the same neural circuit,” *NIPS*, 2013.
- [6] J. C. Venter, M. D. Adams, G. G. Sutton, A. R. Kerlavage, H. O. Smith, and M. Hunkapiller, “Shotgun sequencing of the human genome,” *Science*, vol. 280, pp. 1540–2+, 1998.
- [7] G. Reddy, K. Kelleher, R. Fink, and P. Saggau, “Three-dimensional random access multiphoton microscopy for functional imaging of neuronal activity,” *Nature neuroscience*, vol. 11, pp. 713–720, 2008.
- [8] B. Grewe, D. Langer, H. Kasper, B. Kampa, and F. Helmchen, “High-speed in vivo calcium imaging reveals neuronal network activity with near-millisecond precision,” *Nature Methods*, pp. 399–405, 2010.
- [9] D. Brillinger, “Maximum likelihood analysis of spike trains of interacting nerve cells,” *Biological Cybernetics*, vol. 59, pp. 189–200, 1988.
- [10] F. Rigat, M. de Gunst, and J. van Pelt, “Bayesian modelling and analysis of spatio-temporal neuronal networks,” *Bayesian Analysis*, vol. 1, pp. 733–764, 2006.
- [11] J. Pillow, J. Shlens, L. Paninski, A. Sher, A. Litke, E. Chichilnisky, and E. Simoncelli, “Spatiotemporal correlations and visual signaling in a complete neuronal population,” *Nature*, vol. 454, pp. 995–999, 2008.
- [12] Y. Mishchenko, J. Vogelstein, and L. Paninski, “A Bayesian approach for inferring neuronal connectivity from calcium fluorescent imaging data,” *Annals of Applied Statistics*, 2010.
- [13] S. Song, P. J. Sjöström, M. Reigl, S. Nelson, and D. B. Chklovskii, “Highly nonrandom features of synaptic connectivity in local cortical circuits,” *PLoS Biology*, vol. 3, p. e68, 2005.
- [14] J. W. Lichtman, J. Livet, and J. R. Sanes, “A technical colour approach to the connectome,” *Nat Rev Neurosci*, vol. 9, pp. 417–422, June 2008.
- [15] K. Chung *et al.*, “Structural and molecular interrogation of intact biological systems,” *Nature*, vol. 497, pp. 332–337, May 2013.
- [16] T. Hastie, R. Tibshirani, and J. Friedman, *The Elements of Statistical Learning*. Springer, 2001.
- [17] T. J. Mitchell and J. J. Beauchamp, “Bayesian variable selection in linear regression,” *Journal of the American Statistical Association*, vol. 83, no. 404, pp. 1023–1032, 1988.
- [18] S. Mohamed, K. Heller, and Z. Ghahramani, “Bayesian and L1 approaches to sparse unsupervised learning,” *ICML*, 2012.
- [19] J. Liu, *Monte Carlo Strategies in Scientific Computing*. Springer, 2002.
- [20] Y. Mishchenko and L. Paninski, “Efficient methods for sampling spike trains in networks of coupled neurons,” *Annals of Applied Statistics*, vol. 5, pp. 1893–1919, 2011.
- [21] J. Diebolt and E. Ip, “A stochastic EM algorithm for approximating the maximum likelihood estimate,” tech. rep., Stanford University, 1994.
- [22] C. Bishop, *Pattern Recognition and Machine Learning*. Springer, 2006.
- [23] Y. W. Teh, D. Newman, and M. Welling, “A collapsed variational Bayesian inference algorithm for latent Dirichlet allocation,” in *Advances in Neural Information Processing Systems*, vol. 19, 2007.
- [24] F. Ribeiro and M. Opper, “Expectation propagation with factorizing distributions: A gaussian approximation and performance results for simple models,” *Neural Computation*, vol. 23, no. 4, pp. 1047–1069, 2011.
- [25] J. Tyrcha and J. Hertz, “Network inference with hidden units,” *arxiv*, p. 1301.7274v1, 2013.
- [26] J. Hertz, Y. Roudi, and J. Tyrcha, “Ising models for inferring network structure from spike data,” <http://arxiv.org/abs/1106.1752>, 2013.
- [27] P. Carbonetto and M. Stephens, “Scalable variational inference for Bayesian variable selection in regression, and its accuracy in genetic association studies,” *Bayesian Analysis*, vol. 7, pp. 73–108, 2012.
- [28] I. M. Park and J. W. Pillow, “Bayesian spike-triggered covariance analysis,” in *NIPS*, 2011.

- [29] K. Sadeghi *et al.*, “Monte Carlo methods for localization of cones given multielectrode retinal ganglion cell recordings,” *Network*, pp. 1–25, 2012.
- [30] A. Ramirez and L. Paninski, “Fast inference in generalized linear models via expected log-likelihoods,” *J. Comput. Neurosci.*, 2013.
- [31] U. Kamilov, S. Rangan, A. K. Fletcher, and M. Unser, “Approximate message passing with consistent parameter estimation and applications to sparse learning,” in *NIPS*, pp. 2447–2455, 2012.
- [32] J. H. Huggins and L. Paninski, “Optimal experimental design for sampling voltage on dendritic trees in the low-snr regime,” *Journal of Computational Neuroscience*, vol. 32, no. 2, pp. 347–366, 2012.